Citation for published version:
Smyth, ASM, Young, AM & Di Mare, L 2021, 'Effect of Three-Dimensional Geometry on Harmonic Gust–Airfoil Interaction', *AIAA Journal*, vol. 59, no. 2, pp. 737-750. https://doi.org/10.2514/1.J059661

DOI:
10.2514/1.J059661

Publication date:
2021

Document Version
Peer reviewed version

Link to publication

University of Bath

Alternative formats
If you require this document in an alternative format, please contact:
openaccess@bath.ac.uk

General rights
Copyright and moral rights for the publications made accessible in the public portal are retained by the authors and/or other copyright owners and it is a condition of accessing publications that users recognise and abide by the legal requirements associated with these rights.

Take down policy
If you believe that this document breaches copyright please contact us providing details, and we will remove access to the work immediately and investigate your claim.

Download date: 05. May. 2023

The Effect of 3D Geometry on Harmonic Gust-aerofoil Interaction*

Amanda S. M. Smyth[1]
University of Cambridge, Cambridge CB3 0DY, UK

Anna M. Young[2]
University of Bath, Bath BA2 7AY, UK

and
Luca Di Mare[3]
University of Oxford, Oxford OX1 3PJ, UK

Two-dimensional (2D) strip-theory modelling of unsteady gust-aerofoil interaction is standard practice in many industrial applications, but the limits of applicability of 2D unsteady flow modelling on 3D wing and rotor geometries are not well understood. This paper investigates the effects of 3D geometry features, such as finite span, taper, sweep and rotation, on the unsteady lift response to gusts, and the flow-physical differences between 2D and 3D geometries in unsteady flow. A frequency-domain inviscid vortex lattice model is validated and used for the 3D analysis. The results are compared to unsteady transfer functions from 2D linear analytic theory (e.g. Theodorsen and Sears functions). The study agrees with previous research findings that 3D effects are most significant at low reduced frequencies and low aspect ratios, as well as near the wing tips. The driving cause of 3D response is shown to be the wake vorticity: both streamwise and spanwise components of unsteady wake vorticity must be modelled. The study concludes by investigating whether unsteady response of more complex 3D wing and rotor geometries can be represented by the response of a rectangular wing. The results indicate that this is possible for tapered wings and rotating blades, but not for swept wings.

Nomenclature

A	Influence matrix	R	Hub rotation radius
b	Semi-chord (m)	t	Time
c	Chord (m)	u	Perturbation velocity (m/s)
Cl	Local lift coefficient	U	Local velocity (m/s)
C_L	Total lift coefficient	α	Angle of attack (rad)
F	Force (N)	ρ	Density
k	Reduced frequency	ϵ	Gust amplitude (fraction of freestream velocity)
L	Lift (N)	λ	Taper ratio
m	Number of chordwise lattice panels	ω	Gust frequency (rad/s)
n	Surface normal vector	$\angle$	Phase angle (degrees)
N_b	Number of blades	Γ	Circulation of vortex ring
r	Radius	Ω	Blade rotational frequency (rad/s)

[1] Research Associate, the Whittle Laboratory, Cambridge University Engineering Department.
[2] Lecturer, Department of Mechanical Engineering.
[3] Associate Professor, Department of Engineering Science.
* A version of this paper was presented at AIAA SciTech in San Diego, Jan 2019, paper no. 2019-0899.

Φ	Flow potential
Λ	Sweep angle (degrees)
$C(k)$	Theodorsen function
$C'(k)$	Loewy function
$S(k)$	Sears function

Subscripts

am	Added mass
DW	Downwash
$gust$	Relating to the unsteady gust
$mean$	Mean quantity
N	Normalised by 2D quasi-steady lift
QS	Quasi-steady
Rel	Relative to 2D unsteady lift response
∞	Freestream quantity

Superscripts

^	Amplitude
$'$	Unsteady quantity
$\lvert\ \rvert$	Modulus

I. Introduction

THE problem of aerofoils encountering unsteady flow is common to many engineering applications, from helicopters and unmanned air vehicles to wind and tidal turbines. In all these applications, the calculation of fatigue life, and the design of control algorithms, relies on accurate prediction of the effect of this unsteady flow on the aerofoil loading. In many applications it is common to evaluate unsteady aerodynamic loading through 2D strip-theory methods. In such models, the wings or rotor blades are divided into 2D sections which are assumed to be impermeable and independent from each other. The 2D performance of each section is evaluated, and the results are interpolated along the span. A variety of correction factors exist for three-dimensional flow; these tend to be derived assuming steady flow, but are often applied to unsteady flow conditions. This extrapolation is done without due consideration of the fundamental differences between 2D and 3D unsteady flow, and so can result in significant errors in the prediction of unsteady load response when using strip-theory methods. These errors are demonstrated in this study, which explores the effects of 3D geometry on unsteady aerofoil loading.

Two important differences between 2D and 3D unsteady flow are the presence of unsteady streamwise wake vorticity, and the finite nature of the spanwise wake vorticity. In the majority of past work only one of these differences is considered, and often in a quasi-steady manner. For wind and tidal turbines, Prandtl's tip loss correction is used to account for the loss of lift associated with the streamwise tip vortex [1][2], but the correction is derived for steady flow conditions. In the field of unsteady lifting line theory the unsteady streamwise vorticity is accounted for (e.g. in [3][4]), but the finite spanwise wake vorticity is neglected. This study demonstrates that both the streamwise and spanwise wake vorticity components must be modelled for accurate load calculations, and investigates their role in driving the unsteady lift response.

After a detailed investigation into the behavior of the two components of unsteady wake vorticity, this study will look at the unsteady lift response of more complex geometries. It is possible to show using steady lifting-line theory that the planform of a wing has a relatively small effect on the steady lift, compared to the effects of the finite span [5]. In theory, then, accounting for the effects of finite span in the unsteady lift response may be a sufficient approximation for geometries with varying planforms, or for rotor geometries. This claim will be investigated at the end of this paper, through the analysis of a selection of 3D geometry features – taper, sweep and rotation – the unsteady lift response of which are compared with that of a simple rectangular finite wing.

The scope of this study is solely on the effect of 3D geometry; the effect of spanwise variation in the unsteady inflow is not addressed here. The method of analysis is inviscid vortex lattice modelling, which is capable of first-order estimates of unsteady aerodynamic loading for attached flow. Furthermore, given equivalent conditions (2D flat plate at zero mean incidence) the vortex lattice model exactly replicates the results of classical unsteady aerofoil theory such as the Theodorsen and Sears functions, which are widely used in industry and have been validated experimentally [6][7][8]. By comparing the 3D vortex lattice model with the classical 2D transfer functions, this study demonstrates the effects of 3D geometry features on unsteady lift response, and investigates the role of the 3D wake in driving the differences between 2D and 3D unsteady flow.

II. Background

A. Classical unsteady aerofoil theory

In linear inviscid modelling, the interaction of unsteady flow with a lifting surface changes the lift response from the quasi-steady equivalent, through added mass forces and downwash from the unsteady vortical wake [6]. The added mass is caused by acceleration of the aerofoil potential field, imparting a resultant force on the aerofoil proportional to the time rate-of-change of the aerofoil circulation. The unsteady wake is generated to satisfy Kelvin's theorem of constant circulation in the flow, as the aerofoil circulation changes in response to the changing angle of attack. This wake induces downwash velocity on the aerofoil, imparting unsteady aerodynamic damping, resulting in lowering of the aerofoil lift.

For harmonic gusts, the degree of unsteadiness in the load response is determined by the reduced frequency. The reduced frequency is traditionally given with respect to the semi-chord b [6], but will in this paper be defined by the full chord length, c, such that:

$$k = \frac{\omega c}{U} \tag{1}$$

where $\omega = 2\pi f$ is the gust angular frequency, and U is the relative incident flow velocity at the aerofoil section. This definition of reduced frequency has been used in other recent studies on unsteady aerofoil response, such as by Sequeira and Miller [9]. The reduced frequency is a measure of how many chord lengths a fluid particle travels during a gust wavelength.

In classical aerofoil theory, the aerofoil is modelled as a 2D flat plate at zero mean incidence, assuming inviscid flow. The wake is assumed to leave the trailing edge along the horizontal axis, travelling with the steady freestream velocity, and gust amplitudes are assumed to be small. One of the most commonly-used transfer functions for harmonic flow is the Theodorsen function [10], which models the aerofoil response to pitching and heaving, or to chordwise-uniform gusts. The load response given by Theodorsen to a harmonic gust, acting uniformly along the chord, is:

$$Cl'_{2D} = 2\pi \left[C(k) + i\frac{k}{2}\right] \epsilon e^{i\omega t} \tag{2}$$

Here $C(k)$ is the Theodorsen function, which is expressed in terms of Hankel functions (see e.g. [6] for the full expression for $C(k)$). The variable ϵ gives the gust amplitude, as a fraction of the mean freestream velocity. For sinusoidal gusts, which vary over the aerofoil chord, the Sears function [11] gives the time-varying lift coefficient as:

$$Cl'_{2D} = 2\pi S(k) \epsilon e^{i\omega t} \tag{3}$$

The transfer function $S(k)$ is the Sears function, which is expressed in terms of Bessel functions (see e.g. [6] for the full expression for $S(k)$).

The Theodorsen function is often used in marine, wind and aerospace industries. However, when evaluating unsteady aerodynamic loads in rotor applications, it is necessary to add a modifier to account for the “returning wake” [9][6]. In an application where a wing is rotating, such as a helicopter or a tidal turbine, the wake forms a helical shape downstream of the aerofoil and therefore comes back into close proximity with the aerofoil N_b times per revolution (N_b = number of rotor blades) – see Fig. 1. In unsteady flow a "resonance" condition can appear in the wake, where the downwash from returning wake sheets acts either to increase or decrease the unsteady lift response. Loewy [12] accounted for this effect and developed a modifier to the Theodorsen function – the Loewy function $C'(k)$ (see e.g. [6] for the full expression) – which can replace the Theodorsen function in Eq. 2. The Theodorsen and Loewy functions will be compared to the 3D vortex lattice model later in this study, in order to demonstrate the differences between 2D and 3D unsteady lift response.

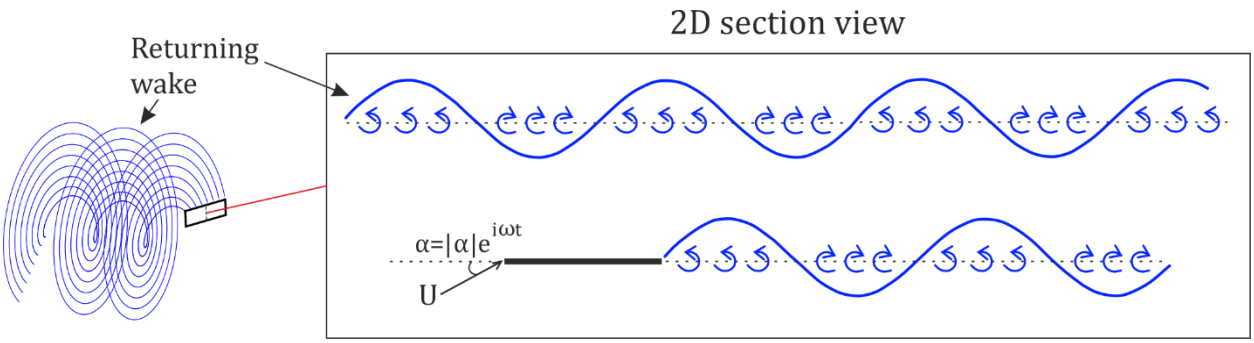

Fig. 1 Illustration of the returning wake behind a single rotating blade, undergoing harmonic gust forcing at frequency ω. The blue arrows in the 2D section view represent harmonically varying wake vorticity.

B. 3D effects and the unsteady wake

While the study of 2D, attached unsteady flow is a mature field, the effects of 3D geometry features on unsteady aerofoil loads are not well understood. Interest in the effects of 3D geometry on unsteady aerodynamic response has been growing recently: Keddington [13] uses CFD simulations to show that an oscillating finite wing gives a different load response from that predicted by 2D or quasi-steady 3D models, and a number of recent studies have studied the effect of finite span and sweep on unsteady aerofoil response, both pre-and post-stall [14][15][16].

Analysis equivalent to that of classical unsteady aerofoil theory is prohibitively complex in 3D, but Namba [17][18] and Schulten [19] developed semi-analytical theories to evaluate 3D unsteady load response in turbomachinery cascades. They found that strip theory deviated strongly from the 3D analysis especially at subsonic (incompressible) and transonic flow speeds. The unsteady response near the blade tips was especially poorly predicted by 2D models. The 3D effects were also found to increase with decreasing blade aspect ratio and decreasing reduced frequency. Namba [18] emphasised the unsteady streamwise wake vorticity as a primary driver for the difference between 2D and 3D unsteady response.

Other studies have also concluded that 2D strip-theory deviates from 3D predictions of unsteady flow response, such as in the prediction of flutter in non-uniform inflow [20][21][22], and in performance predictions for wind turbines [23][24]. The semi-analytical results of Namba and Schulten have been used in validation of 3D unsteady linearized Euler codes for use in turbomachinery cascades [25][26][20], showing that strip theory is not appropriate for use in these applications.

As identified by Namba [18] and others, one of the primary effects of 3D geometry relates to changes to the vortical wake. While the unsteady wake of a 2D aerofoil consists of spanwise vortex lines which are assumed to extend to infinity, an inherent feature of any finite-span geometry is that:

1) The spanwise wake vorticity is finite and may vary along the span.
2) There is also a streamwise component of wake vorticity.

In the past, attempts were made to extend the Theodorsen function to account for finite span or varying planform, by accounting for either the streamwise wake vorticity (e.g. [27][28]) or the finite spanwise wake vorticity (e.g. [29]), but attempts were largely limited to quasi-steady corrections. In later developments, the field of unsteady lifting line theory accounted for 3D effects by using 2D models, such as the Theodorsen function, with the angle of attack corrected to account for the downwash from the streamwise wake vorticity [3][30]. However, unsteady lifting line theory retains the assumption that the spanwise wake vorticity extends infinitely in the spanwise direction, which does not apply for low aspect ratios or in the proximity of the wing tips [31].

Other studies have accounted for the finite spanwise wake vorticity, but do not usually include the unsteady streamwise vorticity. Snel [32] modified the unsteady load model for a wind turbine to account for the fact that the 2D wake was finite in the spanwise direction, but used a quasi-steady assumption for the streamwise wake vorticity. Similar simplifications have been made by others (e.g. [33][34]); if the streamwise wake vorticity is included it is generally assumed to be quasi-steady.

To the authors' knowledge, no study has compared the relative importance of each component of unsteady wake vorticity in generating downwash, and therefore the above simplifications appear to be based on analytical or computational convenience as opposed to physical validation. Motivated by the crucial role of the wake in unsteady aerofoil response, the present study will focus on the behaviour of both the streamwise and spanwise components of unsteady wake vorticity, and will show that they are both important for the unsteady load response of 3D aerofoils.

III. Numerical method

This study uses an inviscid vortex lattice model (VLM) to investigate the effects of 3D geometry features on unsteady aerofoil response. The model was developed by the authors, based on that outlined by Katz and Plotkin [35] with modifications to allow for frequency-domain modelling.

The benefit of frequency-domain modelling is its speed, as the entire time-history of the flow is obtained through a single matrix equation. The analysis is restricted to harmonic gusts, but this does not present a limitation to the present study: the assumption of harmonic flow, or of the linear superposition of harmonic flow components, is common in the evaluation of unsteady gust response (e.g. [9][8]), justifying the use of the harmonic Theodorsen or Sears functions.

Frequency-domain calculations require a pre-existing knowledge of the spatial shape of the wake – a "prescribed wake" – since the wake cannot develop naturally as it would in a time-stepping model. Throughout this study, the wake is assumed to move downstream with the mean flow velocity. This assumption is made throughout 2D classical aerofoil theory and is considered reliable since wake deformation in small-amplitude gusts occurs far enough downstream to have no effect on the aerofoil [6]. For rotor geometries the applicability of this assumption is not as obvious; this will be discussed in relation to the validation of the model in Section III.B.

Blade thickness effects are not included in this study, as these should not affect the inviscid results. Any coupling effects between the aerofoil and the incoming flow are also neglected; the gusts are assumed to convect unchanged through the domain ("frozen gust" assumption).

A. The vortex lattice model

Fig. 2 shows an illustration of the 3D vortex lattice model. The aerofoil is discretised into panels, with associated vortex rings of strength Γ providing the aerofoil circulation – shown in blue in Fig. 2. Each panel has a collocation point at three-quarter chord (red dot), where the boundary conditions are evaluated. This placement of the collocation point implicitly ensures that the Kutta condition is met. The wake is formed when the trailing edge ring vortices are shed into the freestream flow at each time step. Although time-stepping is not required in the frequency-domain, the time step size dt is used as an input variable determining the wake lattice resolution. The circulation of a wake vortex ring is the same as the trailing edge panel circulation at the time when the vortex ring was shed into the freestream, given by $\Gamma_{(\mathrm{jm-i\,dt})}$ (see Fig. 2). Here j indicates spanwise position, m the number of chordwise panels and i the number of time steps that have passed since the wake vortex was shed from the aerofoil.

In order to find the unknown circulation of each vortex ring on the aerofoil, a matrix equation is created based on the boundary condition that the induced flow normal to the aerofoil surface must sum to zero. This boundary condition is applied to each panel collocation point, and the Biot-Savart law is used to find the influence of each panel and wake vortex on each collocation point. The resulting matrix equation has the following form:

$$(\boldsymbol{A\Gamma} + \boldsymbol{U}).\boldsymbol{n} = \left(\boldsymbol{A\Gamma} + \mathbf{U}_\infty + (\boldsymbol{\Omega} \times \mathbf{r}) + \mathbf{u}_{\mathrm{gust}}\right).\boldsymbol{n} = 0 \tag{4}$$

In this notation, $\boldsymbol{U}$ represents the relative velocity at each collocation point, which is the sum of the freestream velocity $\mathbf{U}_\infty$, rotational velocity $(\boldsymbol{\Omega} \times \mathbf{r})$, and the unsteady gust velocity $\mathbf{u}_{\mathrm{gust}}$. The surface normal vector of each panel is denoted $\boldsymbol{n}$. The matrix $\boldsymbol{A}$ is the influence matrix. It contains information about the aerofoil geometry and wake shape and applies the Biot-Savart law to calculate the velocity induced by each vortex on each collocation point, given the vector of vortex circulations $\boldsymbol{\Gamma}$. Because the model is developed in the frequency-domain, the wake-induced velocities

are included in the influence matrix. For a more detailed description of this vortex lattice model and the influence matrix, see [36].

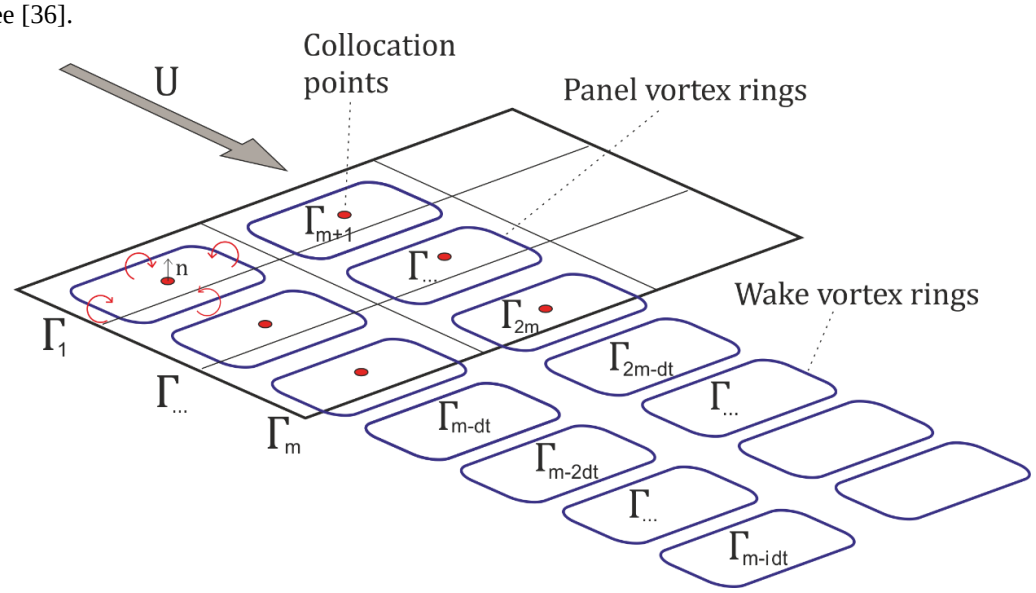

Fig. 2 Structure of the 3D vortex lattice model. Γ represents the circulation of each vortex ring, *n* the normal vector, *m* the number of chordwise lattice divisions, *dt* the time step size and *i* the number of time steps since the wake vortex was shed from the aerofoil.

Inverting the influence matrix in Eq. 4 gives the distribution of panel circulation, **Γ**. With this information the force on each panel can be calculated from the vector form of the Kutta-Joukowski theorem:

$$\boldsymbol{F} = \rho(\boldsymbol{U} \times \boldsymbol{\Gamma}) + \boldsymbol{F}_{am} \tag{5}$$

The parameter $\boldsymbol{F}_{am}$ is the added mass force, obtained from the time derivative of the potential field:

$$\boldsymbol{F}_{am} = \left(\rho \int_0^c \frac{d}{dt} \Delta\Phi\right) \boldsymbol{n} \tag{6}$$

The expression $\Delta\Phi$ is the difference in potential across the top and bottom surfaces of the aerofoil, which for a vortex panel method is equal to the vortex strength at each panel, Γ. The time derivative in Eq. 6 is trivially evaluated by noting that in the frequency-domain the circulation has the form $\Gamma = \hat{\Gamma} e^{i\omega t}$, meaning that:

$$\frac{d\Gamma}{dt} = i\omega\Gamma \tag{7}$$

Lattice resolution studies were performed for all results presented below, such that the unsteady lift amplitude did not change by more than 2% when doubling the resolution. The lowest lattice resolution used for the results presented in Sections IV and V is [26×85] and the highest resolution used is [100×80]. The time step dt is chosen such that the aerofoil panels are at least twice as long in the chordwise direction as the wake vortex rings are in the streamwise direction, since a condition for accuracy in unsteady flow is that the wake is more highly resolved than the blade. The wing and rotor geometries investigated in this paper are illustrated in Fig. 3, with the relevant parameters for aspect ratio (AR), taper ratio (λ), sweep (Λ) and rotation radius (R) defined.

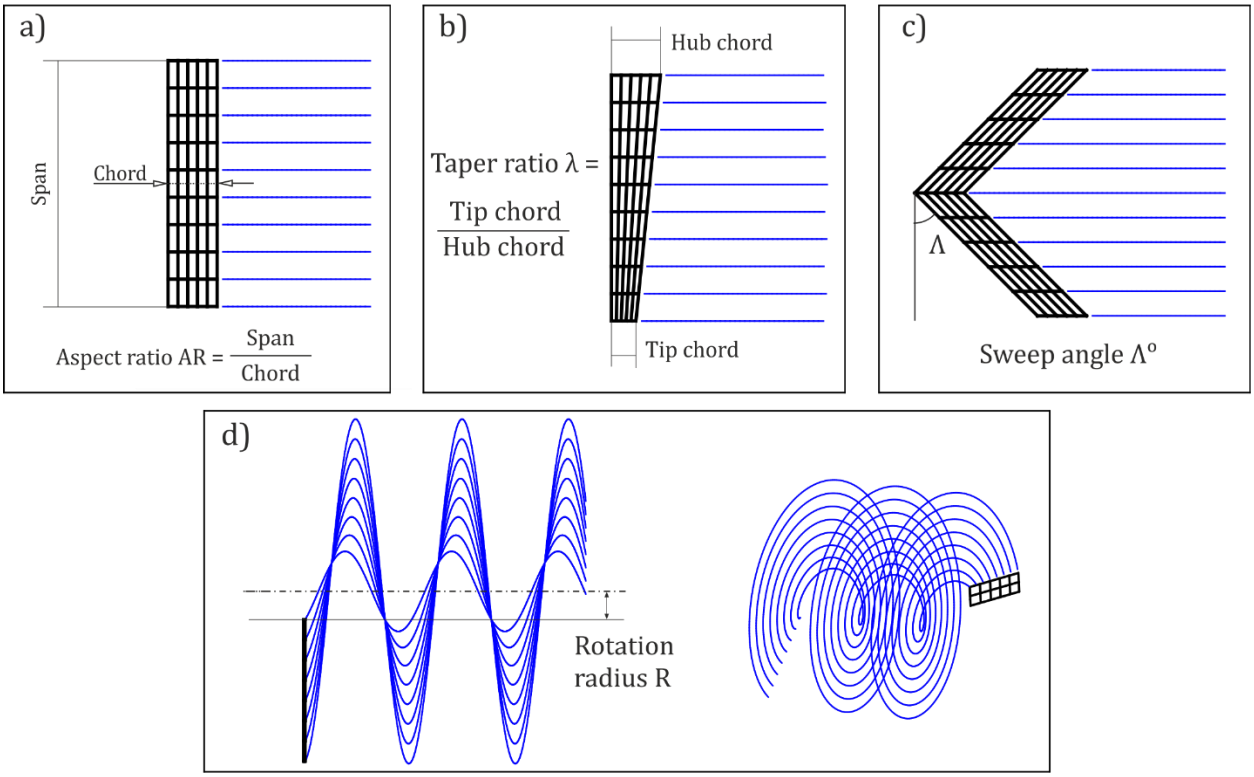

Fig. 3 Definitions of the geometries investigated in this paper. a) Rectangular wings, b) tapered wings, c) swept wings, d) flat-plate rotor blade. The blue lines represent the streamwise wake vorticity.

B. Performance of the vortex lattice model in steady flow

Katz and Plotkin [35] give several validation cases for their steady flow vortex lattice model. These cases were themselves validated against experimental data. Fig. 4 shows a selection of these validation cases for the model introduced in section III.A.

In both Figs. 4a and 4b the local lift coefficient is normalised by the spanwise average value. Fig. 4a shows the spanwise lift distribution of a rectangular wing with aspect ratio 4, at zero sweep, 45° sweep (backward), and -45° sweep (forward). The results from the vortex lattice model (dots) agree with the validation cases (lines). Fig. 4b shows the spanwise lift variation for a wing with aspect ratio 7.28, at different taper ratios (λ). Again, the agreement between the vortex lattice model and the validation cases is good, except at the limit of zero taper ratio ($\lambda = 0.0$ – green line in Fig. 4b). The panel method cannot capture the lift response in this case, since the structure of the model requires that the vortex panels have nonzero length, which is not satisfied for $\lambda = 0.0$. This is however a relatively extreme geometry for both rotor blades and aircraft wings and will not be considered in the present study, and so the tapered wing results in Fig. 4b are satisfactory.

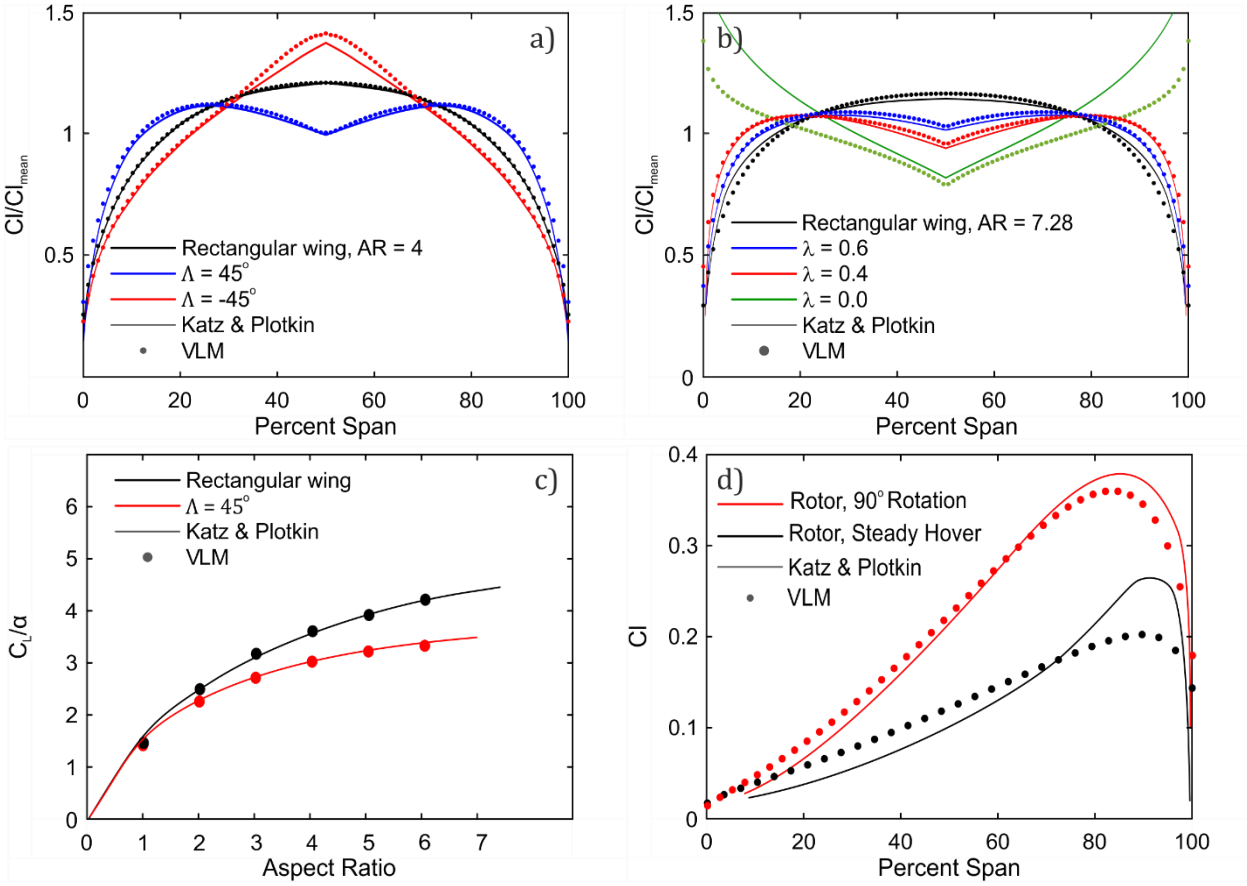

Fig. 4 Steady performance validation of the vortex lattice model. a) Spanwise lift distribution at different sweep angles (Λ). b) Spanwise lift distribution at different taper ratios (λ). c) Lift slope for increasing aspect ratio, with and without sweep. d) Spanwise lift distribution on an impulsively started rotor blade.

Fig. 4c shows the total lift coefficient of rectangular and swept wings with varying aspect ratios, normalised by the angle of attack in radians (effectively giving the lift slope of each wing). Once again, the vortex lattice (dots) shows excellent agreement with validation data (lines) for both swept and unswept geometries with aspect ratios as low as 1.

Fig. 4d shows the case of an impulsively started rotor consisting of two flat plates, again compared with the results obtained by Katz and Plotkin, which were validated against an experimental study by Caradonna and Tung [37]. In the experiment, the aerofoil section is a NACA 0012 profile, which is modelled as a flat plate in this study. Fig. 4d considers two different flow states: an impulsively started rotor that has rotated a quarter of a full rotation (red dots and line), and one that has reached "steady-hover" with a fully-developed wake (black dots and line). The first flow state is replicated well by the vortex lattice model introduced in section III.A, while the agreement is less good in steady-hover conditions. This can be explained by the strong deformation of the fully developed wake of a rotor in hover, which is not included in this study because of the requirement of a prescribed wake (as explained at the start of section III).

The results in Fig. 4d suggest that wake deformation may be an important consideration. However, the discrepancy between the vortex lattice model and the validation data for the steady-hover case in Fig. 4d (black dots and lines) is exaggerated by the absence of steady freestream flow, meaning that the deformed wake remains close to the rotor blades, rather than convecting away. In a separate study on tidal turbine loading, the authors showed that the effects of wake deformation on the turbine loads were small [38], demonstrating that the assumption of a non-deforming wake is adequate for cases where a mean flow causes convection of the wake away from the rotor blades. Later in this

study, when a rotor geometry is considered (Section V.C), a mean flow is always applied and so wake deformation effects are minimised.

C. Replicating classical unsteady aerofoil theory using the vortex lattice model

Unlike the case of 2D aerofoils, there is no established analytic transfer function for predicting the unsteady load response of 3D geometries that can be used for validation of the vortex lattice model. To ensure that the model can capture unsteady aerofoil response, the mid-span response of a high aspect ratio wing (AR = 50) was compared to classical unsteady aerofoil theory (introduced in Section II.A). In Fig. 5 the mid-span response to a sinusoidal and a uniform gust is compared with the Sears and Theodorsen functions (Eq. 2 and 3), respectively. Fig. 5a shows the amplitude and Fig. 5b the phase of the unsteady response, as the reduced frequency of the gust (Eq. 1) increases. The lift amplitude and phase are defined as:

$$|Cl'_N| = \frac{|\hat{L}'|}{0.5\rho U_\infty^2 c[2\pi\epsilon]} \tag{8}$$

$$\angle Cl'_N = \tan^{-1}\left(\frac{Im[\hat{L}']}{Re[\hat{L}']}\right) \tag{9}$$

The unsteady lift L' is obtained from the vortex lattice model, using Eq. 5. The lift amplitude (Eq. 8) is normalized by the quasi-steady lift of a 2D flat plate ($2\pi\epsilon$). The definition of the phase in Eq. 9 means that a positive phase indicates that the load response is leading the gust forcing, while a negative phase indicates that the load is lagging behind the gust.

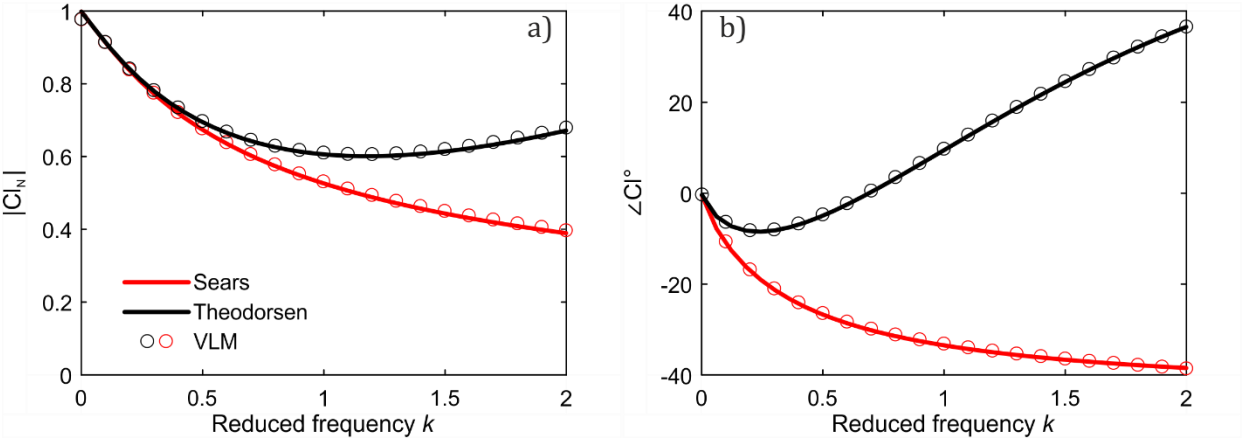

Fig. 5 Unsteady performance validation of the vortex lattice model. a) Amplitude (Eq. 8) and b) phase (Eq. 9) of lift at mid-span of a rectangular wing, AR=50.

Fig. 5 shows that the agreement between the vortex lattice model and classical aerodynamic theory is good, confirming that the model captures the relevant inviscid unsteady flow physics. In a separate study, the vortex lattice model presented in section III.A was also compared to 3D URANS simulations of a tidal turbine [38], to assess the accuracy of the VLM compared to high-order viscous simulation. The VLM predictions of the unsteady turbine loads were within 12% of the CFD, with the majority of the results being within 7%. Importantly, the inviscid and viscous simulations showed the same general trends, confirming the inviscid model's suitability for first-order predictions of unsteady loading.

IV. The effect of finite aspect ratio on harmonic gust response

In this section, the response of finite wings with flat-plate aerofoil sections to harmonic gusts is considered, through vortex lattice modelling of rectangular wings with different aspect ratios (see Fig. 3a). The selection of this highly

simplified geometry is intended to replicate the conditions under which the classical unsteady transfer functions were derived (flat plate, inviscid, zero mean angle of attack) as far as possible; the only change introduced is the finite span.

The gusts applied are harmonic transverse gusts, uniform in the spanwise and chordwise directions, giving the gust velocity over the whole wing as:

$$u_{gust} = \epsilon U_\infty e^{i\omega t} \tag{10}$$

In strip-theory modelling, the load response to this gust would be found using the Theodorsen function (Eq. 2), and so this approach will be compared to the VLM predictions. The results will be displayed as local normalized unsteady lift amplitude and phase (Eq. 8 and 9). It is also relevant to show the results in terms of the lift amplitude and phase relative to the 2D analytic solutions:

$$|Cl_{Rel}| = \frac{|cl'_N|}{|cl'_{2D}|} \tag{11}$$

$$\angle Cl_{Rel} = \angle Cl'_N - \angle Cl'_{2D} \tag{12}$$

Eq. 11 and 12 gives the amplitude and phase relative to the 2D function evaluated at the same reduced frequency. The definition of phase is such that positive relative phase means that the 3D response leads the equivalent 2D response. Showing the relative responses in this way highlights the differences between the 2D and 3D load response at different reduced frequencies and spanwise positions.

A. Unsteady lift on a finite rectangular wing

Fig. 6 shows the lift response at mid-span of rectangular wings with aspect ratios from 1 to 9, computed by the vortex lattice model introduced in section III, when forced by a uniform gust (Eq. 10). The results are compared with the results from the 2D Theodorsen function (Eq. 2 – red line). Fig. 6a shows the normalised lift amplitude (Eq. 8) while Fig. 6b shows the phase (Eq. 9).

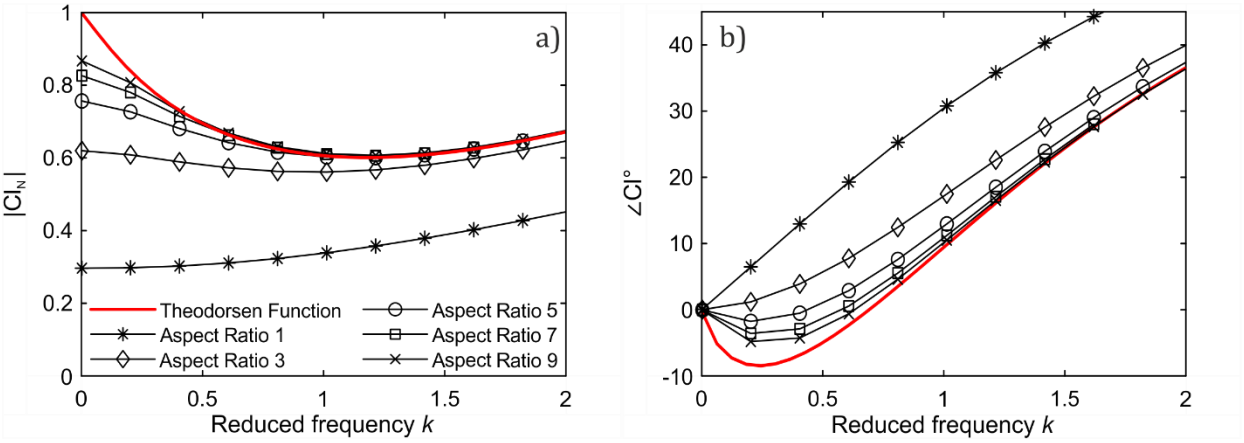

Fig. 6 a) Amplitude (Eq. 8) and b) phase (Eq. 9) of unsteady lift at mid-span of rectangular wings, undergoing uniform gust forcing.

Figure 6a shows that the lift amplitude at zero reduced frequency (quasi-steady) decreases with decreasing aspect ratio. This reduction is explained by the inherent reduction in steady lift in a finite wing caused by the downwash of the streamwise wake vorticity. However, as the reduced frequency increases the 3D lift response gradually approaches the 2D response, in most cases matching it exactly at high frequencies. The rate of this approach decreases with decreasing aerofoil aspect ratio, and the aspect ratio 1 wing has substantially lower amplitudes than the 2D characteristic even at large k, because of the strong influence of the tip vortices at this aspect ratio. As observed by

Namba [18], the effects of the streamwise wake vorticity diminish with increasing k such that the flow is fully captured by 2D models at high reduced frequencies, causing the approach to 2D behavior in Fig. 6. In unsteady lifting line theory this is called "self-cancellation" or "self-averaging" of the streamwise wake [4]. Nevertheless, the influence of the streamwise vorticity remains strong near the wing tips, as will be shown below, which is why the aspect ratio 1 wing remains far from the 2D characteristic throughout the given frequency range.

The phase of the response (Fig. 6b) agrees with the 2D prediction at zero reduced frequency before diverging, and then approaches the 2D characteristic again at high frequencies. The agreement at zero k is expected because the quasi-steady response must, by definition, be in phase with the gust forcing in both 2D and 3D. The 3D phase does not approach the 2D characteristic as rapidly as did the amplitude in Fig. 6a, and fully matches the 2D characteristic only at high aspect ratios and large k. The reason for this will be examined in Section IV.B.

The variation in lift response across the wing span is shown in Figure 7, for a uniform gust at a single frequency $k = 1.0$. The lift amplitude (Fig. 7a) diminishes in proximity of the wing tips for all aspect ratios investigated. As the aspect ratio increases, a larger proportion of the span exhibits 2D behaviour. This is true also for the phase (Fig. 7b), but a smaller proportion of the span is in phase with the 2D response, compared with the load amplitude at the same aspect ratios. Again, the reasons for this will be examined in Section IV.B.

The phase variation in Fig. 7b also shows that the tip response leads the mid-span response, for all aspect ratios. This means that the wing tip and the mid-span do not respond in phase with each other, even when there is no spanwise gust variation.

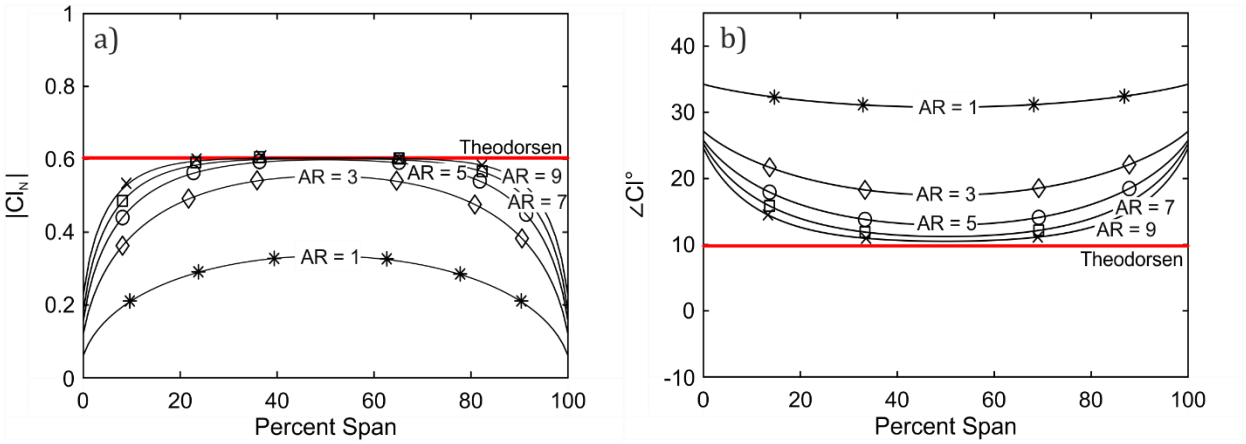

Fig. 7 Spanwise lift distribution of lift a) amplitude (Eq. 8) and b) phase (Eq. 9) for rectangular wings, undergoing uniform gust forcing at reduced frequency $k = 1.0$.

It is important to note that the distribution of unsteady spanwise lift amplitude shown in Fig. 7a is not equal to the quasi-steady lift distribution, i.e. the effect of finite span on loading is dependent on k. As such, it is not possible to obtain the unsteady response of the 3D wing by applying a quasi-steady correction to the Theodorsen function. This can be illustrated by considering the relative lift amplitude and phase (Eq. 11 and 12). Fig. 8 shows the relative lift amplitude (8a) and phase (8b) of an aerofoil with aspect ratio 5 responding to uniform gusts over a range of reduced frequencies. The quasi-steady response is given by $k = 0.0$. As the frequency increases, the lift amplitude approaches the 2D value (the horizontal line at $|Cl_{Rel}| = 1$), as does the phase (approaching 0^o relative phase), everywhere except the region near the wing tips. Clearly, the 3D lift response changes relative to the 2D response as k increases, meaning that a quasi-steady correction is insufficient to capture the effects of finite span on the unsteady lift.

Fig. 6 suggested that the unsteady lift of a finite wing approached the 2D characteristic with increasing k. Fig. 8 shows that this is not the case in the vicinity of the wing tips. The relative lift amplitude (8a) remains virtually unchanged at the tip as k increases, while the phase difference between the 2D and 3D lift response (8b) increases with increasing k. The "self-cancellation" process in the streamwise wake vorticity [4][18], introduced above, appears not to be strong enough to overcome the effect of the streamwise wake vorticity in the vicinity of the wing tips.

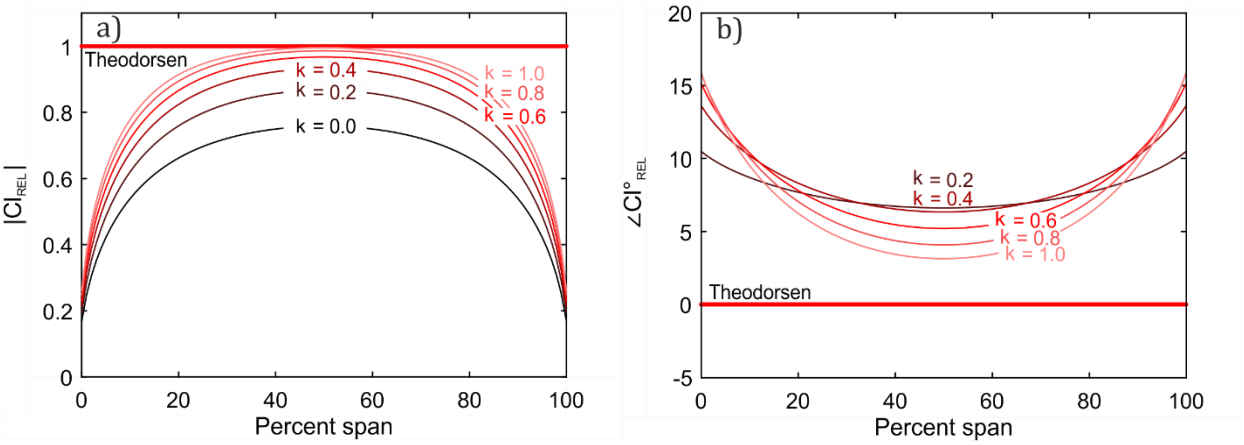

Fig. 8 Spanwise distribution of relative lift a) amplitude (Eq. 11) and b) phase (Eq. 12) for a rectangular wing with AR=5, undergoing uniform gust forcing.

Figs. 6 to 8 suggest the following conclusions, with respect to the impact of finite span on unsteady load response:

1) 3D effects increase with decreasing aspect ratio.
2) 3D effects increase with decreasing reduced frequency.
3) 3D effects are always strong near the tips, regardless of aspect ratio and frequency.

Here "3D effects" are defined as deviation from the 2D prediction for the equivalent blade section. The listed findings agree with observations from previous studies into unsteady 3D effects, such as the semi-analytical studies of Namba [17][18], the numerical study of Hall and Lorence [20] and the experimental results of Green and Smits [39]. Point 1) is also readily observed in steady flow, and the scalability of unsteady flow response with aspect ratio was also shown numerically by Ayancik et. al. for rectangular plates [34].

Note that the results in Figs. 6-8 are all for uniform (Theodorsen-type) gust response (Eq. 10). A similar analysis was performed using sinusoidal (Sears-type) gusts and showed qualitatively similar effects, resulting in the same conclusions as those listed above.

While the above results were obtained using an inviscid linear model, they are expected to remain relevant for viscous load predictions unless a significant portion of the span is stalled. In a separate URANS CFD study on the unsteady loads of a tidal turbine [38] the authors found the inviscid model to predict the same trends as the viscous simulations: the unsteady thrust acting on the turbine approached the 2D prediction at high k, while the unsteady torque did not. This is because the torque is primarily generated near the blade tips, which result in strongly 3D response also at high k, as shown in Fig. 8. The inviscid solver also predicted this trend, and the loads were within 7% of the CFD for the majority of cases, suggesting viscous effects were small compared to inviscid 3D effects.

B. The role of the unsteady vortical wake

The cause of the differences between 2D and 3D lift response shown in Fig. 6-8 can be found by examining the leading-edge downwash induced by the unsteady wake. Downwash counteracts the variations in leading edge incidence and is therefore a measure of the damping of unsteady response provided by the wake, such that a case with larger downwash will have a smaller unsteady load. Fig. 9 shows the magnitude of leading-edge downwash velocity ($|u_{DW}|$) along the span of two wings, one with aspect ratio 5 (Fig. 9a) and one with aspect ratio 9 (Fig. 9b). The downwash is normalised by the gust amplitude ϵU_∞. The gust is uniform (Eq. 10) as in the previous section, and the reduced frequency is $k = 1.0$.

The 2D downwash is shown for comparison as a red line in Fig. 9. In 2D the spanwise wake vorticity is assumed to extend to infinity, and the streamwise wake vorticity does not exist. As such, the 2D downwash is constant across the span. By contrast, the total 3D downwash (thick black line) varies significantly along the span, with a minimum at the mid-span and a maximum at the wing tips.

In order to show the relative importance of the streamwise and spanwise wake vorticity, the downwash induced by each are shown separately; that of the spanwise wake vorticity by a thin black line, and that of the streamwise wake vorticity by a dashed black line. Note that the spanwise and streamwise wake vorticity components are not in phase, so the total downwash is not the sum of the magnitudes of the two components. Because the wing is finite, the spanwise wake vorticity is also finite, and the downwash it generates is at a maximum at the mid-span and significantly reduced near the tips. The streamwise wake vorticity shows the opposite trend – its induced downwash peaks at the wing tips and is lowest at mid-span.

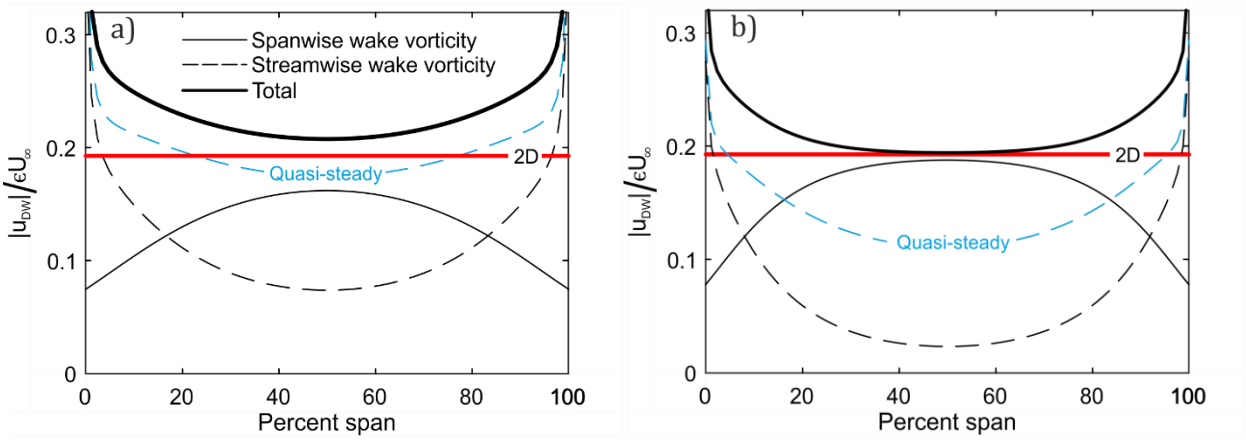

Fig. 9 Amplitude of the unsteady wake downwash (u_{DW}) normalised by the gust amplitude (ϵU_∞), for rectangular wings with a) AR=5 and b) AR=9, both undergoing uniform gust forcing at $k = 1.0$.

In quasi-steady conditions, only streamwise wake vorticity contributes to the downwash in 3D. This is represented by the blue dashed line in Fig. 9. The unsteady behaviour of the streamwise wake vorticity (black dashed line) can be seen by comparing it to the quasi-steady downwash: the magnitude of the downwash induced by the streamwise wake vorticity at $k = 1.0$ is much less than the quasi-steady downwash. The reason for this is the "self-cancellation" of the unsteady streamwise wake [4][18] described in section IV.A, which causes its influence to diminish with increasing k. This is seen more clearly in Fig. 10, which shows the downwash at mid-span against k for the two aspect ratios used in Fig. 9. The figures show that the streamwise vorticity downwash (dashed line) is largest at $k = 0.0$, and then decreases with increasing k. The spanwise vorticity downwash (thin solid line), on the other hand, increases from zero at $k = 0.0$ and has a shallow peak at around $k = 1.0$.

These observations of the nature the streamwise and spanwise wake vorticity explain the unsteady lift response observed in Figs. 6-8 above. The total downwash (thick black line, Fig. 9) is at a minimum at mid-span, and maximum at the wing-tips, so there is more damping and therefore lower unsteady lift near the tips. As k increases, the downwash from the streamwise wake vorticity diminishes, and the spanwise wake vorticity becomes dominant (see Fig. 10). The spanwise downwash approaches the 2D value, and so the unsteady lift approaches the 2D characteristic (as in Fig. 6). However, since the streamwise wake vorticity remains strong at the wing tips, the response here deviates strongly from 2D predictions even at high k (as shown in Fig. 8).

Fig. 10 emphasises the importance of the combined influence of both streamwise and spanwise components of wake vorticity. While the total downwash magnitude is similar for the two aspect ratios at $k > 1.0$, the balance of streamwise and spanwise components differs between the two. The downwash magnitude of the aspect ratio 5 wing (Fig. 10a) is made up of significant contributions from both wake components throughout the frequency range shown, while the aspect ratio 9 wing (Fig. 10b) has a downwash magnitude solely consisting of the spanwise component of wake vorticity when $k > 1.0$. This indicates that while the amplitude of the unsteady lift is approximately 2D for both aspect ratios at $k > 1.0$ (see Fig. 6a), this is caused solely by the spanwise component of wake vorticity for the higher aspect ratio wing, and by a combination of both wake components for the lower aspect ratio case. This adds weight to the argument that it is necessary to include both components of the wake in order to model the unsteady response correctly.

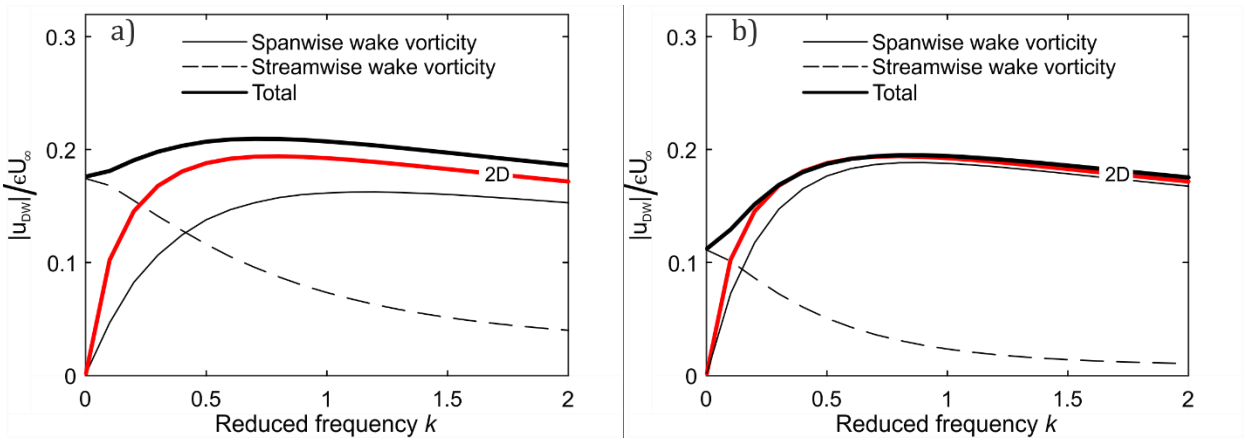

Fig. 10 Leading-edge unsteady wake downwash (u_{DW}) at mid-span, normalised by the gust amplitude (ϵU_∞), for two rectangular wings: a) AR=5, b) AR=9. Both wings are undergoing uniform gust forcing.

In Section IV.A it was noted that the unsteady lift amplitude approached 2D behaviour at lower k than did the phase: Fig. 6b shows that the wing with aspect ratio 9 has the same mid-span phase response as a 2D aerofoil at $k >$ 1.0, but also that the aspect ratio 5 wing does not reach the 2D phase response in the given frequency range. This deviation of the phase response from the 2D prediction, even when the lift amplitude is 2D, appears to occur when the total downwash is caused by a combination of streamwise and spanwise wake vorticity. This is the case for the lower aspect ratio wing in Fig. 10a. The high aspect ratio wing (Fig. 10b), on the other hand, has negligible streamwise vorticity downwash for $k > 1.0$, and the phase approaches that of the 2D case in Fig. 6b. As such, the results indicate that the phase response only approaches the 2D characteristic if the response is entirely caused by the spanwise wake vorticity.

C. Discussion

The most important finding in this section is that for a finite wing the streamwise and spanwise components of wake vorticity can induce downwash of similar magnitude across the majority of the wing span, for all the tested aspect ratios. This is significant because many previous attempts have been made to produce reduced-order models accounting for the changes to the 3D wake in unsteady conditions, but to the authors' knowledge none has accounted for both unsteady components of wake vorticity simultaneously. This is the case in unsteady lifting line theory which assumes the spanwise variation to be negligible (e.g. [3]), and in other models that assume the streamwise wake vorticity to be quasi-steady (e.g. [32][33]). The results in this section show that neither of these assumptions are adequate on their own: the total downwash is a strong function of both the finite spanwise wake vorticity and the unsteady streamwise wake vorticity. This agrees with the recent findings of Ayancik et. al. [34], who showed that both wake vorticity components are important in determining the propulsive efficiency of harmonically pitching rectangular plates, although they assumed a quasi-steady scaling of the streamwise vorticity.

The study in the present paper was carried out assuming inviscid flow and small-amplitude perturbations. For large-scale gust forcing in viscous flow the effects of flow separation are expected to dominate. In this case the interaction of the unsteady wake with separated leading-edge vortices, as in the infinite-wing study by Zurman-Nasution et. al. [40], may be a primary consideration for load prediction. This cannot be captured by the present inviscid model, but the importance of both components of unsteady wake vorticity in generating downwash is expected to remain relevant in viscous and separated flow. An example is the decreasing intensity of dynamic stall near the wing tips due to downwash from the tip vortices, as demonstrated in e.g. [23].

V. The effect of additional 3D geometry features on harmonic gust response

It is known from steady lifting-line theory that the planform of a wing has a relatively small effect on the steady lift, compared with the effects of the finite span [5]. In theory, then, accounting for the finite span alone may give reasonable results for the unsteady lift response of geometries with varying planforms, and even for rotor geometries. This idea will be investigated in this section, for a selection of wing and rotor geometries (see Fig. 3 for geometry definitions). The rotors have flat plate cross-sections and are untwisted, as in the validation case used in Fig. 4d but with added mean axial flow. The rotation of the blade will be given in terms of the tip-speed ratio (TSR), the ratio between the blade tip speed and the steady axial freestream velocity.

A. Tapered wings

The aspect ratio for the tapered wings (Fig. 3b) is determined with respect to mid-span chord (i.e. the 'average' aspect ratio over the wing), and the gust forcing is uniform (Eq. 10). Since the incident velocity is the same at all spanwise positions but the chord varies, the local reduced frequency (Eq. 1) decreases linearly along the span as the chord length decreases. This variation in reduced frequency means that the Theodorsen function must be evaluated at each spanwise section (this gives a local '2D response' as would be predicted by a strip-theory method). Fig. 11a shows the spanwise lift amplitude for a wing with aspect ratio 5 with a range of taper ratios, for mid-span $k = 1.0$. Fig. 11b shows the phase for the same geometries. Each tapered wing has the same aspect ratio of 5, with respect to the mid-span chord. An untapered wing ($\lambda = 1.0$) with the same aspect ratio is included for comparison (thick black line). Note that 0% span corresponds to the portion of the aerofoil with the longest chord while 100% corresponds to the shortest chord section, such that the taper ratio is $c_{100\%}/c_{0\%}$.

Figs. 11a and 11b show an increasing asymmetry in the response with decreasing taper ratio, both for the predicted 2D response (dashed lines) and the 3D response (solid lines). At a first glance, the tapered blade response displays significant differences from the untapered blade. Looking instead at the relative lift amplitude (Fig. 11c) and phase (Fig. 11d), the differences are less dramatic. The relative lift and phase are given by Eq. 11 and 12. While the tapered relative lift response does not collapse entirely onto the untapered lift response, the latter can be considered to be a good approximation. The differences in phase response between the taper ratios are more pronounced, especially for the smallest taper ratio ($\lambda = 0.2$) at 100% span. The maximum discrepancy, however, is less than 10^o, which will yield only small differences to the integrated load, especially as it occurs near the tip where the lift amplitude is small due to tip-loss effects. As such, the relative lift response of an untapered wing is a good approximation of the relative lift response of tapered wings. The assertion that the effects of wing planform are small relative to the effect of a finite span (introduced at the start of Section V) holds for the tapered wing.

The results in Fig. 11 were obtained for uniform gust interaction (Eq. 10). The same analysis was performed for a sinusoidal gust, and the same conclusion was drawn: that the relative lift response for a tapered wing undergoing sinusoidal gust forcing is well represented by the relative response of an untapered wing in the equivalent gust conditions. The requirement is that the tapered and untapered wings have the same aspect ratio.

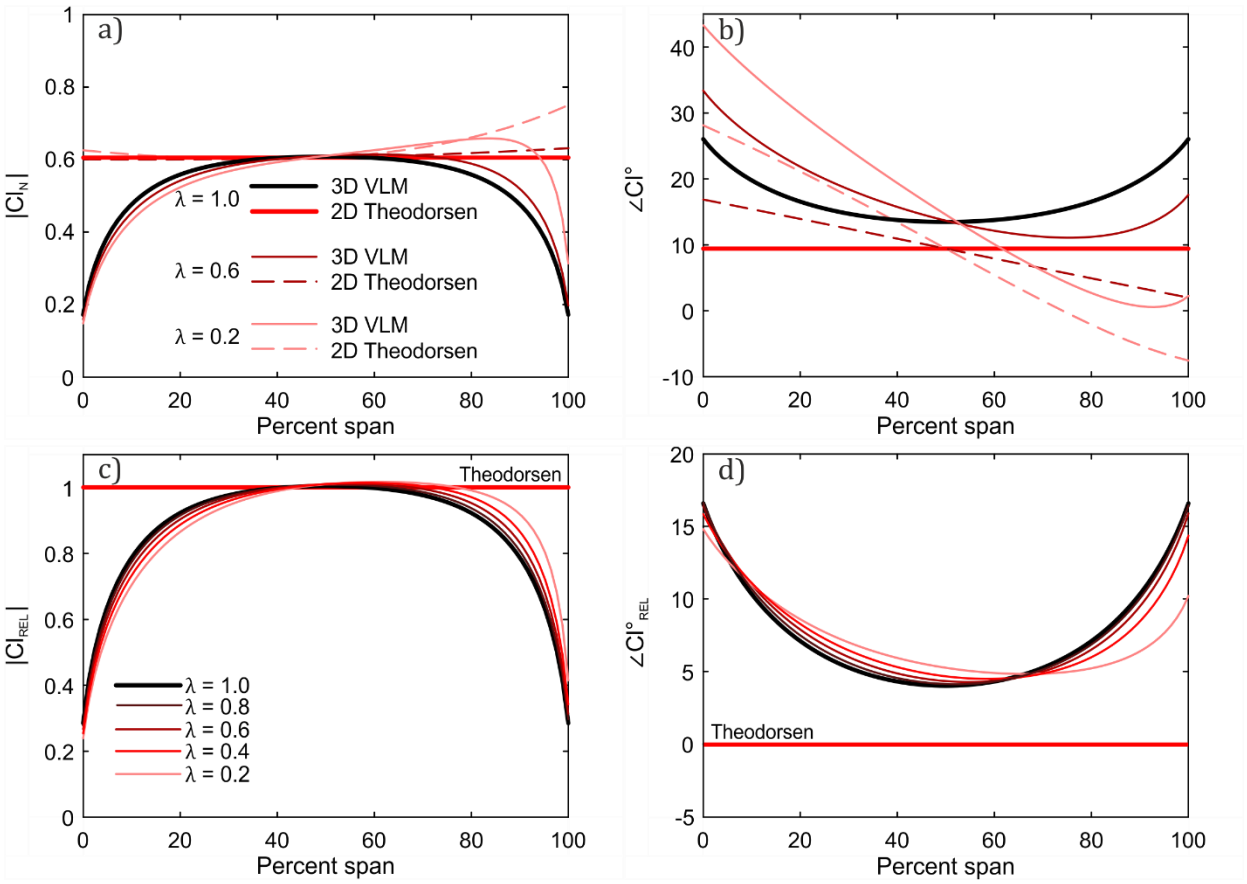

Fig. 11 Spanwise distribution of lift for varying taper ratios (λ), all AR=5, in uniform gust forcing at mid-span $k = 1.0$. a) Amplitude (Eq. 8), b) phase (Eq. 9), c) relative lift amplitude (Eq. 11) and d) relative phase (Eq. 12).

B. Swept wing

We will now investigate the effect of sweep (Fig. 3c) on the unsteady load response. The chord length at every spanwise station is defined in the streamwise direction, meaning that the reduced frequency is constant along the span and is identical for swept and unswept wings with the same aspect ratio (for a given gust frequency ω and freestream velocity U). Because the gust is uniform with no spatial variation (see Eq. 10), it acts in-phase across the span of both swept and unswept wings, meaning that any difference between the two is due to the sweep angle rather than any spanwise variation in the gust properties.

Fig. 12 shows the relative lift response (Eq. 11 and 12) for a 45° backward-swept wing, in terms of relative amplitude (12a) and phase (12b), and for a -45° forward-swept wing, again in terms of relative amplitude (12c) and phase (12d). The response is shown relative to the 2D prediction by the Theodorsen function (horizontal red line), and can be compared to Fig. 8 which shows the behaviour of an unswept wing with the same aspect ratio.

The behaviour of the swept wings in Fig. 12 is substantially different from the unswept wing in Fig. 8. While the unswept wing gradually approaches the 2D response with increasing k, the swept wings remain highly 3D for all frequencies shown. The amplitude (12a and 12c) does not approach the 2D response at any point along the span, and the phase (12b and 12d) only marginally so at approximately quarter-span. As such, the swept wing response is not well approximated by an equivalent unswept wing. Accounting only for finite span effects is insufficient, and the unique response of the swept geometry must be fully accounted for. The theory presented at the start of Section V – that accounting for finite span is more important than the wing planform – does not hold for swept wings.

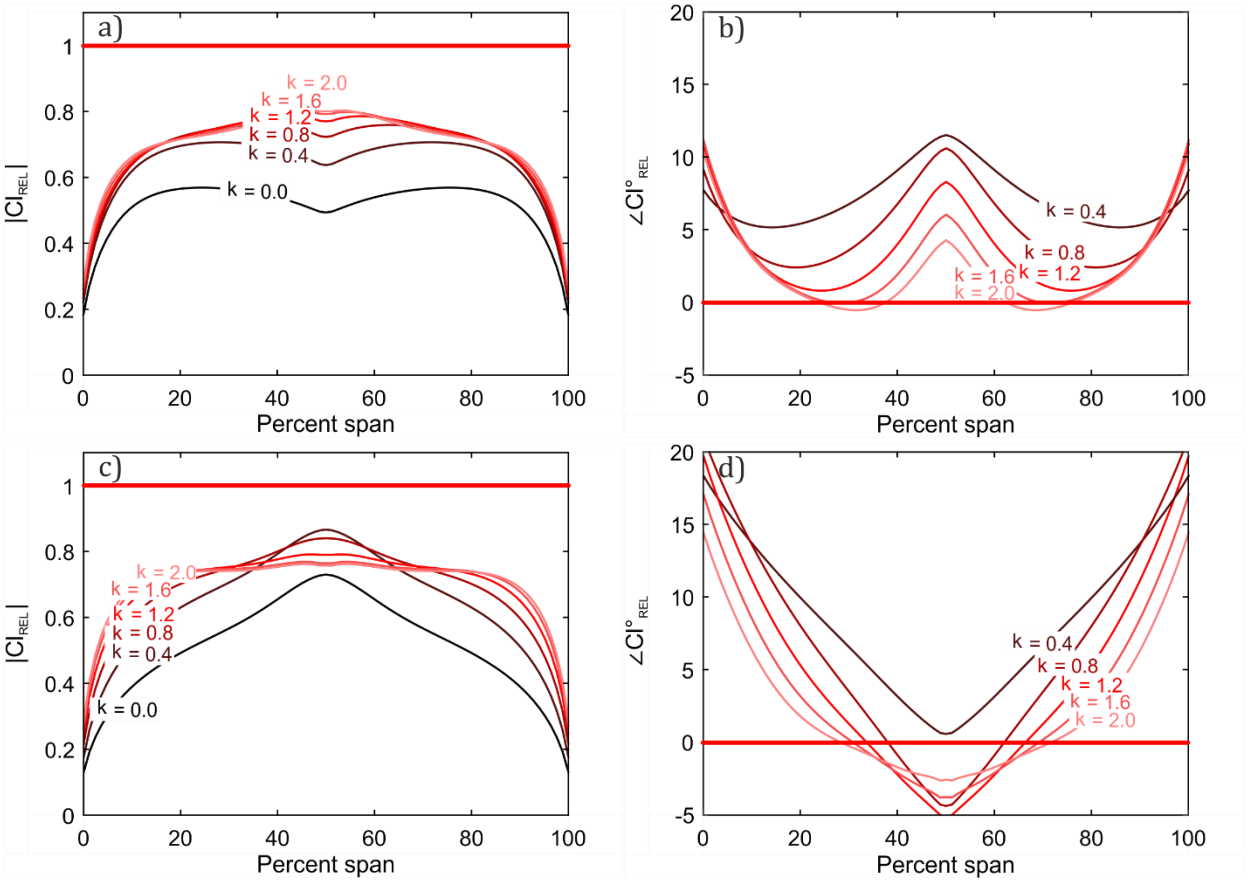

Fig. 12 Relative lift for symmetric swept wings (AR=5) undergoing uniform gust forcing. Sweep angles: Λ=45º a) amplitude (Eq. 11) and b) phase (Eq. 12), and Λ= -45º c) amplitude (Eq. 11) and d) phase (Eq. 12).

C. Rotor with flat-plate cross-section

As a final example, we investigate the unsteady load response of a single rotor blade to uniform gust forcing (Eq. 10), with the gust acting in the axial flow direction – see Fig. 3d for geometry. This configuration results in a transverse uniform gust in the relative frame of the blade sections. The rotor cross-section is a flat plate of constant chord that is untwisted along the span (as in the validation case used in Section III.B, Fig. 4d).

One consequence of the blade rotation is that the reduced frequency k (Eq. 1) varies along the span, as it did in the case of the tapered wing in Section V.A. For the rotating blade, the spanwise variation in k is not linear, but is inversely proportional to the radial location r:

$$k = \frac{\omega c}{\left[U_\infty^2 + (\Omega r)^2\right]^{1/2}} \tag{13}$$

Here Ω is the rotational speed of the blade. Three different rotor hub radii will be considered below: $R = 10 \times$span, $R = 1 \times$span and $R = 0.2 \times$span. The largest hub radius results in a relatively small spanwise variation in k, but as the hub radius decreases the spanwise variation in k increases and becomes more nonlinear.

To assess how well the unsteady lift response of a rotating blade can be accounted for by finite-span effects only, Fig. 13a shows the unsteady lift amplitude and Fig. 13b the phase of the three blades rotating at different radii, and of a non-rotating blade with the same aspect ratio. The gust frequency ω is chosen in each case such that the mid-span k of each rotating blade is equal to that of the non-rotating blade (for which k is uniform across the span), at $k = 2.0$. Fig. 13c and 13d shows the same results in terms of relative lift response (Eq. 11 and 12). The high value of k was

chosen such that returning wake effects (see Section II.A) are negligible, meaning that the Theodorsen function can be used to represent the 2D response in Fig. 13.

Looking at Fig. 13a and 13b, the differences between the rotating and non-rotating cases seem significant, apart from the case with the largest hub radius ($R = 10 \times$span), which matches the non-rotating blade – this is expected, since the effects of rotation decrease with increasing rotation radius. However, the agreement in the relative lift response (Eq. 11 and 12) in Fig. 13c and 13d is much better. There are small differences in relative load amplitude (Fig. 13c), especially for the smallest hub radius ($R = 0.2 \times$span), but the non-rotating case is a good approximation of the unsteady load amplitude of the rotating blades. The agreement in relative phase (Fig. 13d) is less good, especially for the smallest hub radius, where the hub leads the tip by 15-20°. In terms of the total load response of the blades, however, this is a minor effect, changing the integrated loads by only a few per cent. For a conservative estimate of the total load, the phase can be assumed to be uniform across the span.

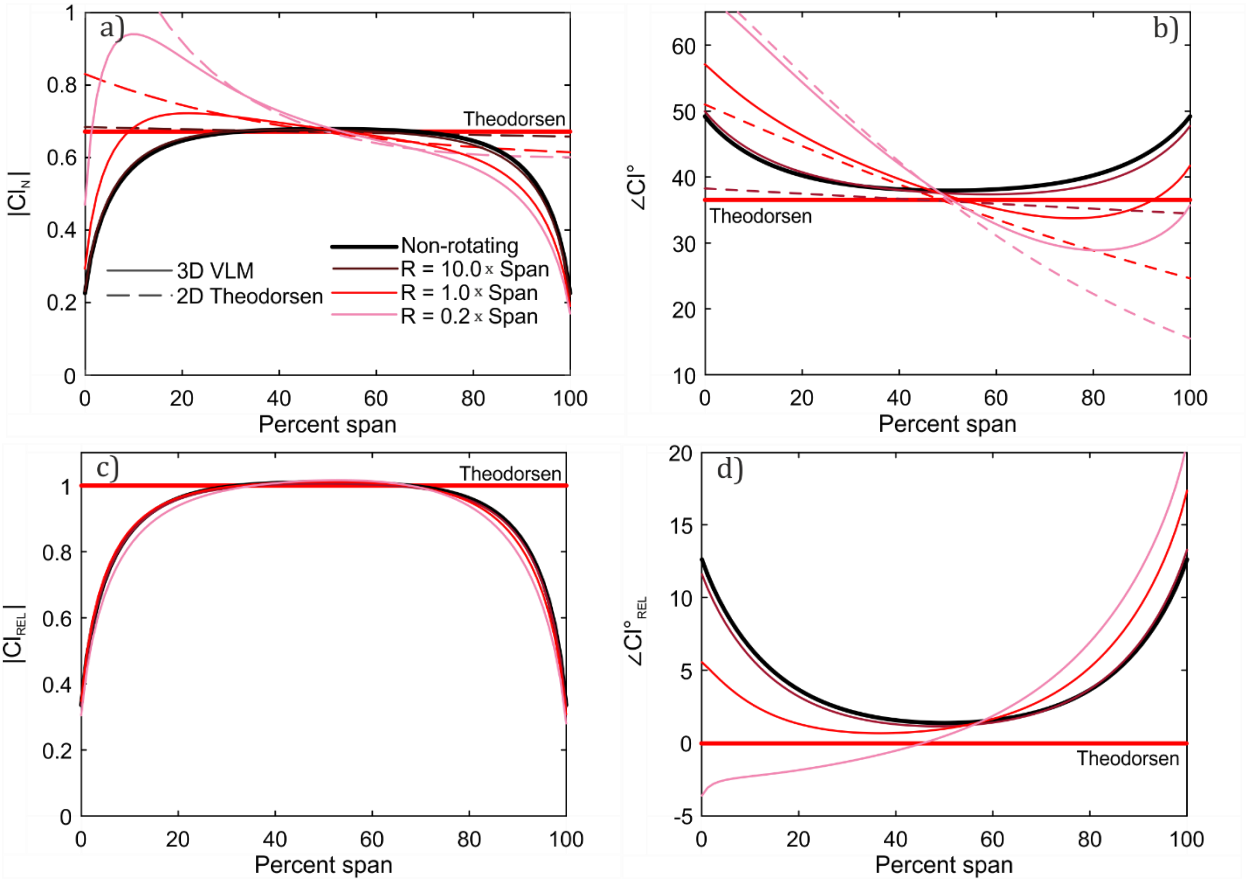

Fig. 13 Lift response for the rotors in Fig. 15, for uniform gust forcing at mid-span k=2.0. a) Amplitude (Eq. 8), b) phase (Eq. 9), c) relative lift amplitude (Eq. 11) and d) relative phase (Eq. 12).

Fig. 13c and 13d suggest that the unsteady response of the rotating blades can be estimated simply by accounting for the finite span, if the results are expressed in terms of the relative lift (Eq. 11 and 12). The same conclusion was found for the tapered wing in Section V.A.

All cases in Fig. 13 are evaluated for mid-span $k = 2.0$. At this frequency returning wake effects are small and need not be accounted for. At lower values of k, returning wake effects are important and can be predicted using the Loewy function in 2D [12]. Fig. 14 shows the mid-span lift response of the rotor blade with hub radius $R = 0.2 \times$span against mid-span k, at three different values of TSR (blade rotation speed relative to axial inflow velocity), in order to investigate returning wake effects on the 3D rotor geometry. Returning wake effects will increase with increasing

TSR, because the wake remains closer to the blade for longer. The left column of Fig. 14 shows the lift amplitude (Eq. 8), while the right column shows the relative lift amplitude (Eq. 11).

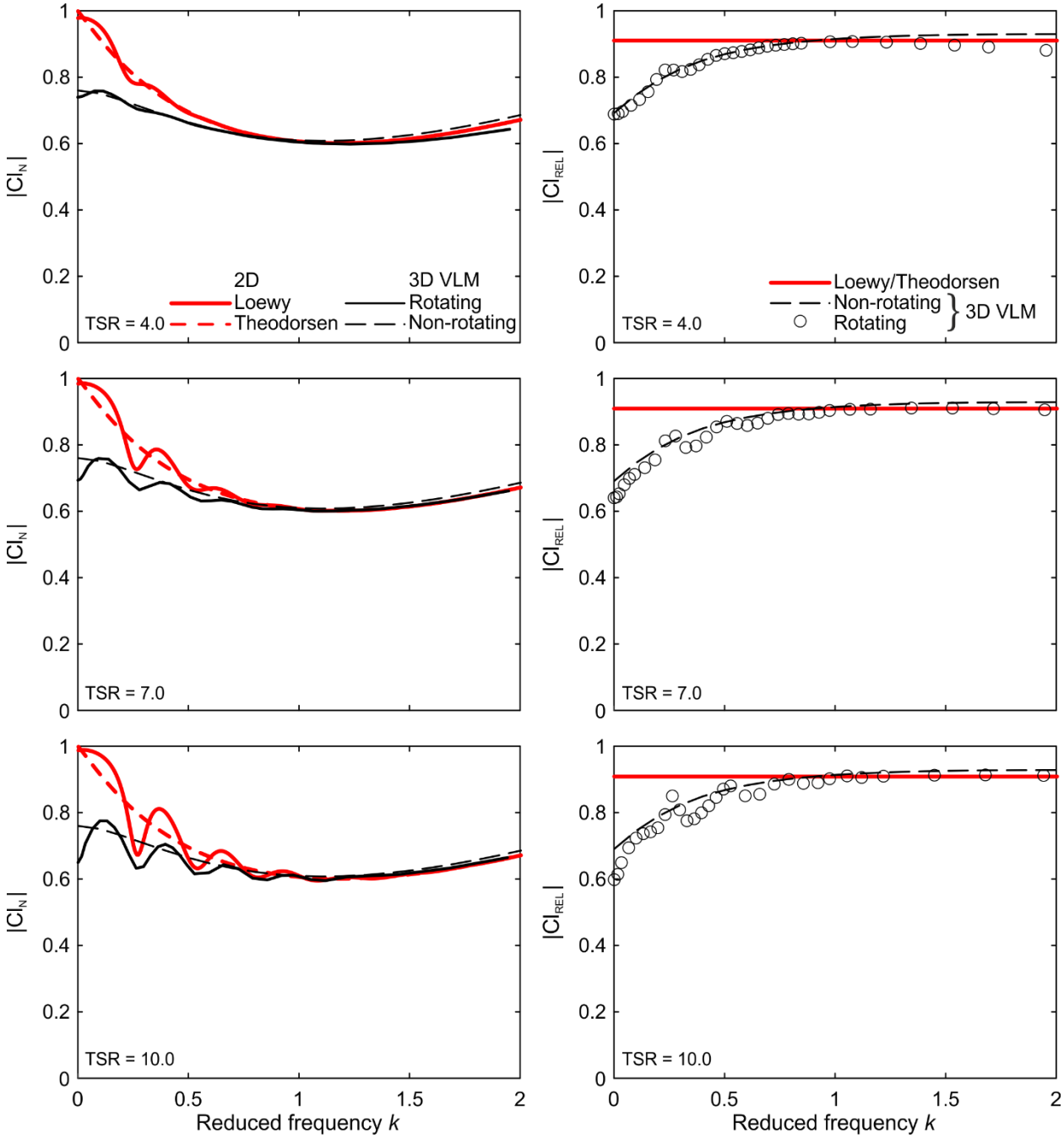

Fig. 14 Lift at mid-span of a rotor blade (R = 0.2×Span, AR=5) undergoing uniform gust forcing, with a non-rotating wing included for comparison. Left column: lift amplitude (Eq. 8). Right column: relative lift amplitude (Eq. 11).

It is clear from the left column of Fig. 14 that returning wake effects tend to be most pronounced at low reduced frequencies, where 3D effects are also most significant. As such, the lift amplitude is consistently over-predicted by the Loewy function. However, the locations of the peaks and troughs in the lift response are quite well predicted, meaning that the wake resonance effect is captured by the 2D function. The Theodorsen function is also included for illustration in the left column of Fig. 14 (dashed red line); the returning wake effects, as predicted by the Loewy

function, result in variation about a mean value given by the Theodorsen function. Similarly, the lift of the 3D rotor (solid black line) appears to vary about the mean value given by the 3D non-rotating lift (dashed black line). This suggests that the wake resonance effects are the same in 3D as in 2D.

The relative lift response is considered in the right column of Fig. 14, for a non-rotating wing (black line) and the rotating blade (circles) relative to the Theodorsen and Loewy functions, respectively. If the response of the rotating blade can be approximated by that of the non-rotating finite wing, the relative lift of the two cases should agree (the circles should lie on the black line), and the agreement in Fig. 14 is quite good. There are however some deviations caused by the fact that the peaks and troughs of the returning wake response do not occur at quite the same k in 2D and 3D (see left column of Fig. 14). These errors are quite small however, meaning that the relative lift of the rotating blade is well approximated by the relative lift of the non-rotating wing of the same aspect ratio. This is the same result as found in Fig. 13 and for the tapered blade in section V.A.

The results in Fig. 14 show again that the finite span is by far the most important aspect to account for among the unsteady 3D effects, and therefore that the unsteady lift response of a rectangular finite wing can be used to approximate the response of more complex geometries, if the results are expressed in terms of the relative lift response (Eq. 11 and 12). Moreover, the returning wake effects in 3D are relatively well captured by the 2D Loewy function, with some small deviations.

VI. Conclusions

As a result of this study, a number of observations can be made about the effect of 3D geometry on the unsteady response of aerofoils. Firstly, some general rules for the importance of 3D effects (and therefore the applicability or otherwise of 2D models) are:

1) 3D effects increase with decreasing aspect ratio.
2) 3D effects increase with decreasing reduced frequency, k.
3) Near the wing or blade tips 3D effects are always significant, irrespective of frequency and aspect ratio.

The listed findings agree with observations from previous studies into unsteady 3D effects (e.g. [18][20][39]). An exception to point 1) and 2) was observed for swept wings (Section V.B), for which the response did not approach the 2D characteristic at any k.

The role of the vortical wake in driving the 3D response was explored by studying the wake downwash, and by dividing it into two components induced by the spanwise and streamwise wake vorticity, respectively. In 2D models the spanwise wake is assumed to extend uniformly to infinity, while the streamwise wake is not included at all. In unsteady flow, the influence of the streamwise wake vorticity diminishes with increasing k due to "self-cancellation". Because of this, the local lift response on 3D wings approaches the 2D characteristic as k increases. An exception is the response near the wing tips, where the streamwise wake vorticity remains strong even at high k, and the influence of the spanwise component of wake vorticity is reduced due to its finite extent. Because of this, the unsteady lift response near the wing tips does not converge on the 2D result even at high k and large aspect ratios. The streamwise and spanwise vorticity components were both found to induce downwash over the majority of the span for all aspect ratios tested, suggesting that the unsteady behavior of both components must be accounted for when evaluating unsteady loads.

In steady conditions, the effect of a finite span is usually more significant to the lift than the planform of the wing or blade [5]. This appears often to be the case also in unsteady conditions. The effects of taper and rotation on the unsteady lift response could be approximated by the response of a rectangular, non-rotating wing, if the results are expressed in terms of the relative lift response (Eq. 11 and 12). This was also the case when returning wake effects are significant, if the lift is obtained relative to the 2D Loewy function. An exception was found in the case of swept wings, where the relative lift response was not well represented by a non-swept wing with the same aspect ratio. Still, the above results suggest that to capture the unsteady response of complex 3D geometries, it may be sufficient to account for the effect of the finite span, while neglecting any second-order planform variation. This opens up possibilities for the development of accurate low-order modelling tools for 3D unsteady aerodynamic loads.

Acknowledgments

The authors would like to gratefully acknowledge the members of the NATO AVT-282 group for their support and feedback throughout this study. We also thank Dr Carl Sequeira and Prof. Rob Miller for their help in establishing the foundations of this project. The research was funded by a Doctoral Training Award (DTA) provided by the UK Engineering and Physical Sciences Research Council (EPSRC).

References

[1] T. Burton, D. Sharpe, N. Jenkins, and E. Bossanyi, *Wind Energy Handbook*. Chichester, England: John Wiley & Sons, 2001, doi: https://doi.org/10.1002/9781119992714.

[2] H. Glauert, *Airplane Propellers*. Berlin, Heidelberg: Springer, 1935, doi: https://doi.org/10.1007/978-3-642-91487-4_3.

[3] P. D. Sclavounos, "An unsteady lifting-line theory," *Journal of Engineering Mathematics*, vol. 21, pp. 201–226, 1987, doi: https://doi.org/10.1007/BF00127464.

[4] J. L. Guermond and A. Sellier, "A unified unsteady lifting-line theory," *Journal of Fluid Mechanics*, vol. 229, pp. 427–451, 1991, doi: https://doi.org/10.1017/S0022112091003099.

[5] H. Glauert, *The Elements of Aerofoil and Airscrew Theory (Cambridge Science Classics)*, 2nd ed. Cambridge: Cambridge University Press, 1983, doi: https://doi.org/10.1017/CBO9780511574481

[6] G. J. Leishman, *Principles of Helicopter Aerodynamics (Cambridge Aerospace Series)*, 2nd ed. Cambridge: Cambridge University Press, 2006.

[7] N. J. Wei *et al.*, "Insights into the periodic gust response of airfoils," *Journal of Fluid Mechanics*, vol. 876, pp. 237–263, 2019, doi: https://doi.org/10.1017/jfm.2019.537.

[8] R. Sankaran and E. D. Jancauskas, "Direct measurement of the aerodynamic admittance of two-dimensional rectangular cylinders in smooth and turbulent flows," *Journal of Wind Engineering and Industrial Aerodynamics*, vol. 41, no. 44, pp. 601–611, 1992, doi: https://doi.org/10.1016/0167-6105(92)90469-Q.

[9] C. L. Sequeira and R. J. Miller, "Unsteady gust response of tidal stream turbines," in *2014 Oceans - St. John's*, 2014, pp. 1–10, doi: https://doi.org/10.1109/OCEANS.2014.7003026.

[10] T. Theodorsen, "General Theory of Aerodynamic Instability and the Mechanism of Flutter," *Naca Report No. 496*, 1935.

[11] W. R. Sears, "Some Aspects of Non Stationary Airfoil Theory and its Practical Application," *Journal of the Aeronautical Sciences*, vol. 8, no. 3, pp. 104–108, 1941, doi: https://doi.org/10.2514/8.10655.

[12] R. G. Loewy, "A Two-Dimensional Approximation to the Unsteady Aerodynamics of Rotary Wings," *Journal of the Aeronautical Sciences*, vol. 24, no. 2, pp. 81–92, 1957, doi: https://arc.aiaa.org/doi/10.2514/8.3777.

[13] M. Keddington, "Computational Fluid Dynamics Simulations of Oscillating Wings and Comparison to Lifting-Line Theory," Thesis, Utah State University, 2015.

[14] A. Medina, M. Rockwood, D. J. Garmann, M. R. Visbal, and A. Ahmed, "On the Characteristics of Three-Dimensional Dynamic Tip Stall on a Swept Wing," in *AIAA SciTech Forum*, 2019, doi: https://doi.org/10.2514/6.2019-2324.

[15] G. Sedky, A. R. Jones, and F. D. Lagor, "Lift modeling and regulation for a finite wing during transverse gust encounters," in *AIAA SciTech Forum*, 2019, doi: https://doi.org/10.2514/6.2019-1146.

[16] C. J. Barnes and M. R. Visbal, "Computational Investigation of the Effect of Sweep on Parallel Vortical-Gust/Wing Interactions on a Finite Aspect-Ratio Wing," in *AIAA SciTech Forum*, 2019, doi: https://doi.org/10.2514/6.2019-0896.

[17] M. Namba and K. Toshimitsu, "Double Linearization Theory of Three-Dimensional Cascades With Vibrating Blades Under Spanwise-Nonuniform Mean Loading, I : Subsonic Flow," *Journal of Sound and Vibration*, vol. 148, no. 1, pp. 41–68, 1991, doi: https://doi.org/10.1016/0022-460X(91)90820-A.

[18] M. Namba, "Three-dimensional flows," in *AGARD Manual on Aeroelasticity in Axial-Flow Turbomachines. Volume 1. Unsteady Turbomachinery Aerodynamics*, Editors: Platzer, M.F. and Carta, F. O. North Atlantic Treaty Organization, Advisory Group for Aerospace Research and Development, 1987, pp. 4.1-4.29.

[19] J. B. H. M. Schulten, "Sound Generated by Rotor Wakes Interacting with a Leaned Vane Stator," *AIAA Journal*, vol. 20, no. 10, pp. 1352–1358, 1982, doi: https://doi.org/10.2514/3.51195.

[20] K. C. Hall and C. B. Lorence, "Calculation of Three-Dimensional Unsteady Flows in Turbomachinery Using the Linearized Harmonic Euler Equations," *ASME Journal of Turbomachinery*, vol. 115, no. 4, pp. 800–809, 1993, doi: https://doi.org/10.1115/1.2929318.

[21] V. Golubev, H. Atassi, and A. Lipatov, "3-D unsteady effects in annular cascades with swirl and comparison with 2-D strip theory," in *3rd AIAA/CEAS Aeroacoustics Conference*, 1997, pp. 400–410, doi: https://doi.org/10.2514/6.1997-1634.

[22] J. M. R. Graham, "Lifting Surface Theory for the Problem of an Arbitrarily Yawed Sinusoidal Gust Incident on a Thin Aerofoil in Incompressible Flow," *Aeronautical Quarterly*, vol. 21, no. 2, pp. 182–198, 1970, doi: https://doi.org/10.1017/S0001925900005357.

[23] F. Balduzzi, J. Drofelnik, A. Bianchini, G. Ferrara, L. Ferrari, and M. S. Campobasso, "Darrieus wind turbine blade unsteady aerodynamics: a three-dimensional Navier-Stokes CFD assessment," *Energy*, vol. 128, pp. 550–563, 2017, doi: 10.1016/j.energy.2017.04.017.

[24] A. Muñoz-Simón, A. Wynn, and R. Palacios, "Unsteady and three-dimensional aerodynamic effects on wind turbine rotor loads," in *AIAA Scitech Forum*, 2020, doi: https://doi.org/10.2514/6.2020-0991.

[25] G. A. Gerolymos and I. Vallet, "Validation of 3-D Euler Methods for Vibrating Cascade Aerodynamics," *ASME Journal of Turbomachinery*, vol. 118, no. 4, pp. 771-782, 1996, doi: https://doi.org/10.1115/1.2840933.

[26] D. Prasad and J. M. Verdon, "A three-dimensional linearized Euler analysis of classical wake/stator interactions: validation and unsteady response predictions," *International Journal of Aeroacoustics*, vol. 1, no. 2, pp. 137–163, 2002, doi: https://doi.org/10.1260/147547202760236941.

[27] E. C. Yates, "Modified-strip-analysis method for predicting wing flutter at subsonic to hypersonic speeds.," *Journal of Aircraft*, vol. 3, no. 1, pp. 25–29, 1966, doi: https://doi.org/10.2514/3.43702.

[28] J. G. Barmby, H. J. Cunningham, and I. E. Garrick, "Study of Effects of Sweep on The Flutter of Cantilever Wings," *NACA Report No. 1014*, 1951.

[29] N. P. Hobbs, "The Transient Downwash Resulting From the Encounter of an Airfoil With a Moving Gust Field," *Journal of the Aeronautical Sciences*, vol. 24, no. 10, pp. 731–740, 1957, doi: https://doi.org/10.2514/8.3955.

[30] A. R. Ahmadi and S. E. Widnall, "Unsteady lifting-line theory as a singular perturbation problem," *Journal of Fluid Mechanics*, vol. 153, pp. 59–81, 1985, doi: https://doi.org/10.1017/S0022112085001148.

[31] H. J. Bird, S. Otomo, K. K. Ramesh, and I. M. Viola, "A Geometrically Non-Linear Time-Domain Unsteady Lifting-Line Theory," in *AIAA Scitech 2019 Forum*, 2019, doi: https://doi.org/10.2514/6.2019-1377.

[32] H. Snel, "Application of a Modified Theodorsen Model to the Estimation of Aerodynamic Forces and Aeroelastic Stability," in *European Wind Energy Conference*, 2004.

[33] J. Boutet and G. Dimitriadis, "Unsteady Lifting Line Theory Using the Wagner Function for the Aerodynamic and Aeroelastic Modeling of 3D Wings," *Aerospace*, vol. 5, no. 92, 2018, doi: https://doi.org/10.3390/aerospace5030092.

[34] F. Ayancik, Q. Zhong, D. B. Quinn, A. Brandes, H. Bart-Smith, and K. W. Moored, "Scaling laws for the propulsive performance of three-dimensional pitching propulsors," *Journal of Fluid Mechanics*, vol. 871, pp. 1117–1138, 2019, doi: https://doi.org/10.1017/jfm.2019.334.

[35] J. Katz and A. Plotkin, *Low-Speed Aerodynamics (Cambridge Aerospace Series)*, 2nd ed. Cambridge: Cambridge University Press, 2001, doi: https://doi.org/10.1017/CBO9780511810329.

[36] A. S. M. Smyth, "Three-Dimensional Unsteady Hydrodynamics of Tidal Turbines," Thesis, University of Cambridge, 2019, doi: https://doi.org/10.17863/CAM.48853.

[37] F. X. Caradonna and C. Tung, "Experimental and Analytical Studies of a Model Helicopter Rotor in Hover," *Nasa Technical Memorandum No. 81232*, 1981.

[38] A. S. M. Smyth and A. M. Young, "Three-Dimensional Unsteady Hydrodynamic Modelling of Tidal Turbines," in *13th European Wave and Tidal Energy Conference, EWTEC*, 2019, doi: https://doi.org/10.17863/CAM.40077.

[39] M. A. Green and A. J. Smits, "Effects of three-dimensionality on thrust production by a pitching panel," *Journal of Fluid Mechanics*, vol. 615, pp. 211–220, 2008, doi: 10.1017/S0022112008003583.

[40] A. N. Zurman-Nasution, B. Ganapathisubramani, and G. D. Weymouth, "Influence of three-dimensionality on propulsive flapping," *Journal of Fluid Mechanics*, vol. 886, 2020, doi: 10.1017/jfm.2019.1078.